Processing and Application of Ceramics 19 [1] (2025) 84–93
https://doi.org/10.2298/PAC2501084A

Sinterability and electrical characterization of $BaCe_{0.9}Y_{0.1}O_{3-\delta}$: A discussion on intrinsic liquid-phase mechanisms

Huyra Estevao de Araujo*

Federal Institute of Education, Science, and Technology of Sao Paulo, Brazil

Received 17 December 2024; Received in revised form 12 March 2025; Accepted 18 March 2025

Abstract

Yttrium-doped barium cerate ($BaCe_{0.9}Y_{0.1}O_{3-\delta}$, BCY) powders were synthesized via two powder processing routes: i) the conventional solid-state reaction and ii) modified wet chemical method. The influence of sintering schedules on densification mechanisms, microstructural evolution and electrical properties was systematically investigated. The results indicate that the intrinsic liquid-phase assisted sintering occurs in the samples prepared by both routes, but it is more prominent for the low-sinterability powder synthesized by solid-state reaction, leading to a more uniform microstructure and conductivity less dependent on sintering conditions. Electrical conductivity measurements revealed that the ceramics prepared via the wet chemical route exhibited superior proton conductivity at lower sintering temperatures, though with more significant variability depending on the processing conditions. The competition between solid-state and liquid-phase sintering significantly impacts densification and electrical performance. These findings highlight the critical role of processing routes and intrinsic liquid phase in tailoring the microstructure and optimizing the electrical properties of the BCY ceramics for electrochemical applications.

Keywords: *barium cerate, proton conductor, liquid phase sintering, electrical conductivity*

I. Introduction

The increasing global demand for sustainable energy and growing environmental concerns related to pollutant emissions have driven extensive research into clean energy sources. Among these, electrochemical devices, such as solid oxide fuel cells (SOFCs), have emerged as promising candidates due to their high efficiency, fuel flexibility and broad range of applications [1]. However, achieving efficient SOFC operation at intermediate temperatures (500600 °C) remains a major challenge, requiring significant improvements in the electrolyte performance, particularly in terms of chemical stability and ionic conductivity [2–5].

In this context, proton-conducting ceramics have gained considerable attention as an alternative to traditional oxygen-ion conductors, such as yttria-stabilized zirconia (YSZ), which typically requires higher operating temperatures [6,7]. Materials based on doped barium cerate ($BaCeO_3$) and barium zirconate ($BaZrO_3$) perovskites have shown significant potential due to their ability to operate at intermediate temperatures while maintaining high proton conductivity [8,9]. However, these materials face distinct challenges: barium cerate exhibits excellent sinterability and high conductivity, but suffers from poor chemical stability in CO_2- and H_2O-containing atmospheres, forming insulating secondary phases [10,11]. In contrast, barium zirconate demonstrates superior chemical stability, but is hindered by its refractory nature, which results in poor sinterability and resistive grain boundaries [12,13].

To address these limitations, hybrid compositions, such as $Ba(Zr,Ce)O_{3-\delta}$ (BCZ), have been developed, aiming to balance the chemical stability of zirconate with the higher proton conductivity of cerate [14]. Despite these advances, the successful implementation of these materials depends on the processing and sintering techniques, which directly affect their microstructure and electrochemical properties [15–17].

Among the various rare-earth dopants, yttrium has been identified as particularly effective in optimizing $BaCeO_3$-based ceramics. Gu *et al.* [18] demonstrated that Y-doped $BaCeO_3$ exhibits the highest electrical conductivity among Ln-doped compositions (Ln = Gd,

* Corresponding authors: tel: +55 19 998863777,
e-mail: *huyraestevao@ifsp.edu.br*

Y, Yb), with sinterability and thermodynamic stability closely linked to the dopant ionic radius. Matskevich *et al.* [19] further reported that the smaller ionic radii in rare-earth dopants contributes to the increased thermodynamic stability in $BaCeO_3$. Yttrium has an intermediate ionic radius and offers an optimal balance between conductivity and structural stability, leading to the improved crystalline symmetry and oxygen vacancy formation. These factors facilitate proton conduction while enhancing sinterability and mitigating phase degradation, establishing Y^{3+} as the most effective doping ion for these barium-based ceramics [8,15,20].

The sintering process is critical in fabricating dense and homogeneous ceramic electrolytes, directly influencing grain growth, densification and overall performance. Barium zirconate-based ceramics often require high sintering temperatures (>1600 °C), which not only complicates processing, but can also lead to barium evaporation and compositional changes [21,22]. In contrast, barium cerate demonstrates intrinsically high sinterability, though the mechanisms underlying this behaviour remain unclear [23]. Recent studies have explored strategies to improve sinterability, including the use of sintering aids such as Cu, ZnO and CuO, which facilitate densification via liquid-phase sintering (LPS) [12,20,21,24]. These sintering aids form transient liquid phases that reduce the sintering temperature or enhance mass transport at grain boundaries [25]. However, adding such aids can sometimes introduce resistive phases or reduce proton conductivity [11].

Alternative sintering techniques, such as two-step sintering (TSS), rapid heating and quenching, have also been investigated to control grain growth and optimize densification profiles [26]. Moreover, choosing powder synthesis routes is crucial in determining the sinterability of proton ceramic conductors and their final microstructure. Chemical routes such as sol-gel and the Pechini method produce fine, homogeneous powders that sinter efficiently at lower temperatures, whereas solid-state reactions typically result in coarser powders that depend more heavily on liquid-phase mechanisms for densification [10].

Despite significant progress, a systematic understanding of the intrinsic sinterability of barium cerate, particularly in the absence of sintering aids, is still lacking. Phase diagrams for pure $BaCeO_3$ suggest the potential for liquid-phase sintering even without dopants, driven by an eutectic reaction within the BaO-CeO_2 system. Understanding this intrinsic behaviour is essential to optimize sintering parameters and correlate them with densification dynamics, microstructural evolution and resulting proton conductivity. Ramos *et al.* [16] suggested a mechanism based on the intrinsic liquid phase for sintering yttrium-doped barium cerate ceramics and its dependence on the powder morphology.

In this work, the sintering dynamics of barium cerate are systematically investigated using various sintering profiles, including fast heating rates and different powder synthesis methods. The aim is to correlate the sinterability of powders and the influence of intrinsic liquid phases on densification, microstructure development and proton conductivity.

II. Experimental

2.1. Sample preparation

The $BaCe_{0.9}Y_{0.1}O_{3-\delta}$ (BCY) ceramic powders were prepared using two distinct methods: i) wet chemical process based on the amorphous citrate method and ii) conventional solid-state reaction. In the wet chemical process, high-purity starting materials, including $Ba(NO_3)_2$, $Ce(NO_3)_3 \cdot 6\,H_2O$ and $Y(NO_3)_3 \cdot 4\,H_2O$ (all supplied by Sigma-Aldrich), were used. Appropriate stoichiometric amounts of each raw material were dissolved in deionized water along with citric acid and hydroxyethyl cellulose (HEC) to obtain a homogeneous and transparent solution. Citric acid acts as a chelating agent, forming metal-carboxyl complexes that enhance the chemical homogeneity of the precursor solution, while hydroxyethyl cellulose (HEC), a high molecular weight polymer, improves dispersion and prevents agglomeration. In this work, the molar ratio of citric acid to total metal cations was maintained at 2:1, and HEC was added at 0.5 wt.% relative to the total solution volume, ensuring uniform distribution of the chelated metal ions throughout the polymeric network. The resulting solution was heated at 400 °C to decompose organic compounds and remove volatile components while preventing premature crystallization. This temperature maintains a homogeneous distribution of metal cations in the precursor powder. Subsequently, the obtained powder was calcined at 1000 °C.

For the solid-state reaction, stoichiometric amounts of $BaCO_3$, CeO_2 and Y_2O_3 were mixed using ball milling for 20 h in an alcoholic medium, employing zirconia grinding media with a ball-to-powder weight ratio of 5:1, according to previous works, to ensure homogeneity [16]. In the next step, the obtained powder was calcined at 1000 °C.

The obtained powders were uniaxially pressed at 200 MPa and the prepared pellets were sintered in the air under two distinct conditions: i) regular and ii) fast heating schedule. In the regular heating schedule, samples were heated at 13.3 °C/min to temperatures ranging from 1250 to 1550 °C, with dwell times of 1 and 10 h. The two heating rates, differing by two orders of magnitude, were chosen to explore distinct sintering dynamics and their effects on densification and microstructure evolution. In the fast heating schedule, the pellets were rapidly inserted into a preheated furnace at 1550 °C, resulting in an effective heating rate of approximately 1000 °C/min, followed by a dwell time of 1 h. Additionally, both powders were subjected to a fast sintering schedule, where the pellets were rapidly heated to 1550 °C, held for 15 min and then quenched to investigate the formation of a liquid phase during sintering.

The reduction of stoichiometric deviations, associated with the high volatility of barium at temperatures approaching 1600 °C, was prevented by surrounding sintering pellets with a powder bath of the same composition during sintering.

2.2. Sample characterization

Crystalline phases of the calcined powders and sintered bodies were analysed by X-ray diffraction (XRD) using a Siemens D5000 diffractometer with CuKα radiation. Measurements were performed in the 2θ range between 5° and 90°, with a step size of 0.01° and a measurement time of 2.5 s/°. The elemental compositions of barium, yttrium and cerium oxides in both the powders and sintered samples were evaluated by X-ray fluorescence (XRF) to verify their agreement with the nominal stoichiometry.

The density of the sintered samples was determined using the Archimedes' method, while the green density of the pellets was measured based on their dimensions. Additionally, green bodies obtained from both powders were sintered in a dilatometer to analyse their linear shrinkage behaviour during sintering. The theoretical densities (TD) were determined from the crystalline structure data obtained via XRD.

The microstructure of the sintered samples was investigated using scanning electron microscopy (SEM) with Philips XL30 FEG and FEI Inspect 80 instruments. Both fractured and polished surfaces were analysed, with thermal etching performed at 50 °C below the sintering temperature to reveal grain boundaries and promote the exudation of any reincorporated liquid phases.

The samples were prepared for electrical characterization by applying Ag paste to both sides of each pellet and firing at 750 °C for 12 min to ensure adhesion while its porosity enhances gas diffusion and charge transfer for impedance spectroscopy. The samples were treated in a wet atmosphere at 600 °C for 2 h to ensure adequate hydration. Electrical conductivity was measured by impedance spectroscopy in wet-to-form porous electrodes air using an HP 4192A impedance analyser. Measurements were conducted from 600 to 100 °C, with

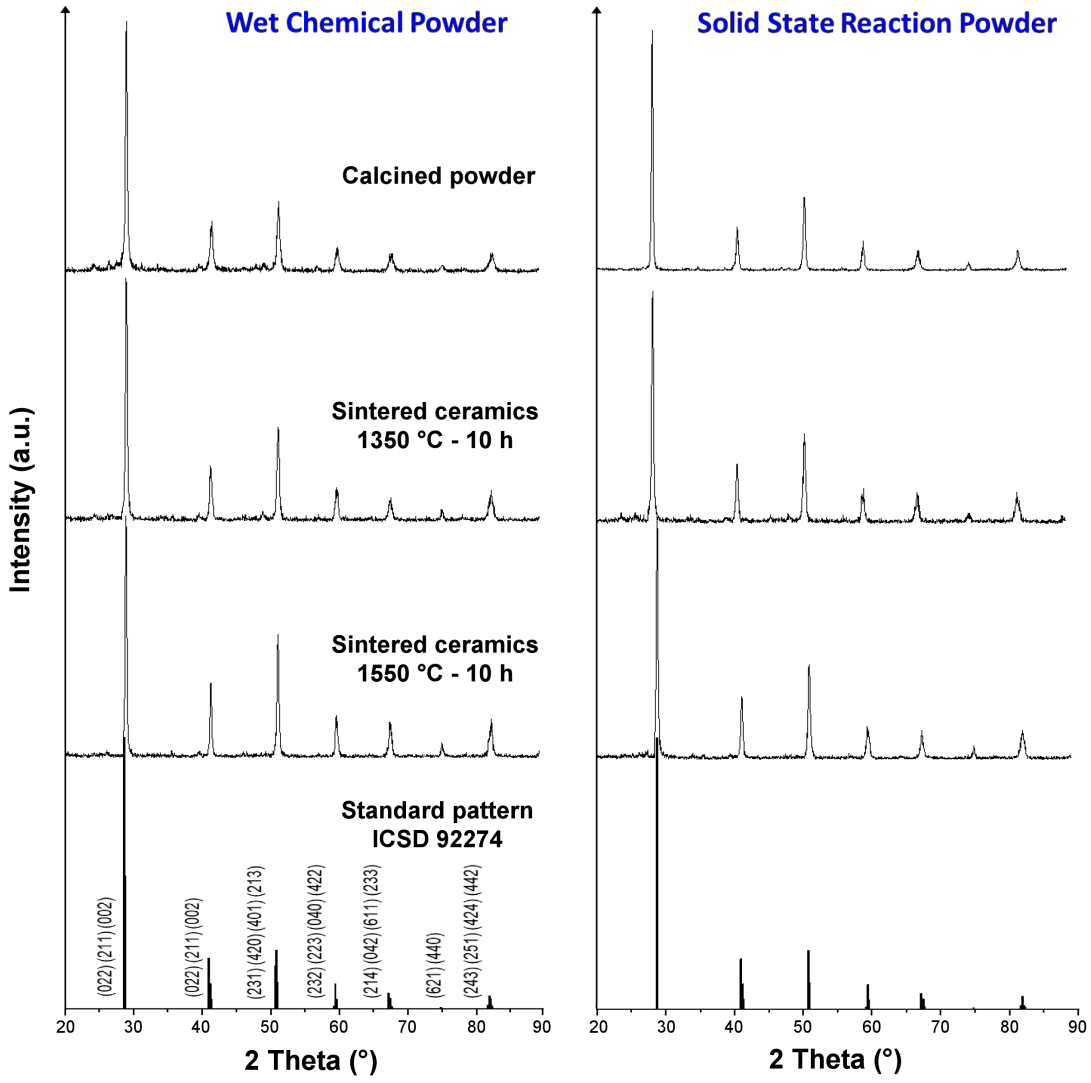

Figure 1. XRD patterns of sintered samples at 1550 °C under different heating conditions (regular and fast heating), compared to ICSD 92274 orthorhombic structure [27]

frequencies scanned from 5 Hz to 13 MHz. The resulting impedance spectra were analysed to distinguish the contributions of bulk conductivity and grain boundary conductivity.

III. Results and discussion

3.1. Phase and chemical composition

Figures 1 and 2 present XRD patterns of the calcined ceramic powders and sintered pellets prepared under various conditions. A comparison with the standard diffraction pattern confirms that both calcined powders crystallized into the The $BaCe_{0.9}Y_{0.1}O_{3-\delta}$ perovskite phase before sintering. Importantly, no substantial secondary phases, often associated with barium loss or the precipitation of cerium and yttrium oxides, were detected, regardless of dwell time or heating rate.

While minor peaks are observable, their presence aligns with the literature data [18,26], which reports that the perovskite phase can exhibit multiple symmetries and undergo complex phase transitions under different thermal conditions. A detailed investigation of these transitions is beyond the scope of this work. The results confirm that the calcination step was sufficient to achieve the desired crystalline perovskite phase, as observed in both powder processing routes.

X-ray fluorescence (XRF) results for the ceramic powders prepared by both processing routes and the ceramic pellets sintered at 1550 °C for 10 h are shown in Fig. 3. The results confirm no substantial deviation in the barium, cerium and yttrium content, even at the highest sintering temperature (1550 °C) and the longest dwell time (10 h). This consistency can be attributed to the usage of the powder bath during sintering, which effectively mitigated barium loss, as reported by Subramaniyan *et al.* [28]. Based on this observation, it is reasonable to assume that temperatures below 1550 °C and shorter dwell times do not result in significant barium volatilization or compositional deviations.

After calcination, the pellets prepared by pressing from both powders have densities of approximately 55 %TD (percentage of theoretical density). This initial

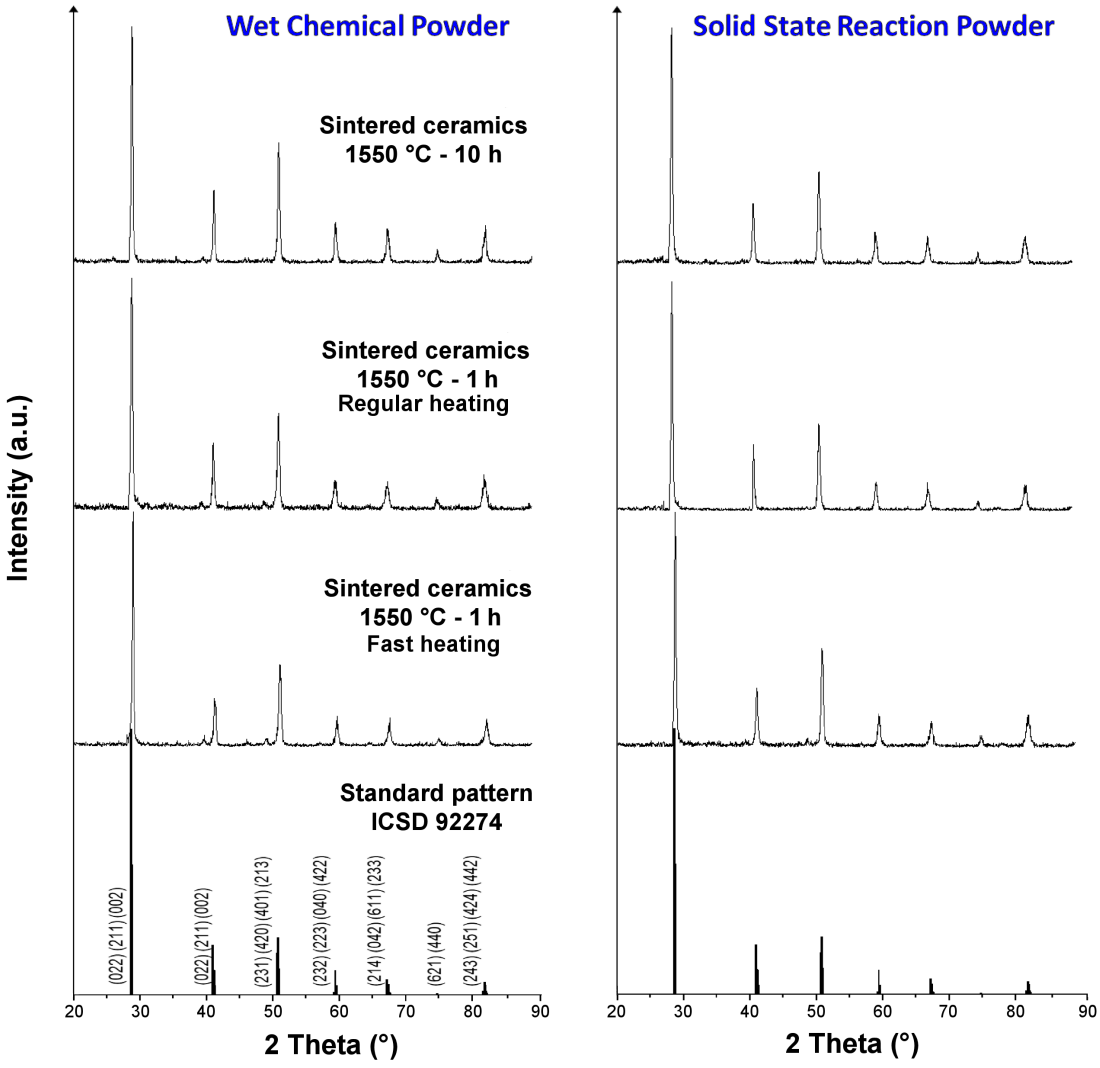

Figure 2. XRD patterns of sintered samples at 1550 °C under different heating conditions (regular and fast heating), compared to ICSD 92274 orthorhombic structure [27]

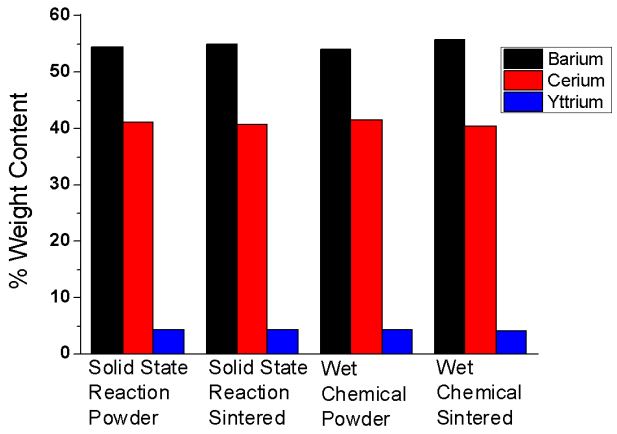

Figure 3. XRF results for ceramic powders prepared by wet chemical and solid-state methods and pellets sintered at 1550 °C for 10 h

density provides a consistent baseline for evaluating the sintering behaviour and densification mechanisms under the various thermal schedules applied in subsequent experiments.

3.2. Sintering behaviour

Figure 4a shows the densities of the ceramic pellets sintered at temperatures ranging from 1250 to 1550 °C for 10 h. The samples prepared by both powder preparation routes achieved densities exceeding 95 %TD at temperatures starting from 1450 °C. Notably, a pronounced increase in density was observed in the ceramics prepared by the solid-state reaction method compared to those synthesized via the wet chemical route. This abrupt densification enhancement might be an indication of liquid-phase-assisted sintering (LPS), characterized by the intrinsic liquid phase facilitating mass transport at elevated temperatures [29].

Figure 4b presents the linear shrinkage profiles of green bodies obtained through dilatometric analysis. The results reveal a distinct sintering behaviour of the solid-state reaction powder characterized by a rapid dimension reduction at approximately 1100 °C, suggesting the onset of liquid-phase formation. This rapid reduction is also visible for the sample obtained from the wet-chemical powder, but less pronounced. Beyond 1400 °C, the shrinkage rate stabilizes and the retraction becomes uniform, indicating the completion of the primary densification stage and the transition to grain growth dominance. It can be concluded that the powders produced through wet chemical synthesis demonstrate gradual and more consistent densification, which is predominantly governed by solid-state diffusion mechanisms due to their finer particle size and higher compositional homogeneity.

Loganathan *et al.* [30] extensively reviewed densification phenomena involving transient liquid phases induced by sintering additives. In contrast, Ramos *et al.* [16] reported similar densification effects in additive-free $BaCe_{0.9}Y_{0.1}O_{3-\delta}$ ceramics, attributing intrinsic liquid-phase formation mechanism. This intrinsic liquid formation, restricted to high-temperature sintering conditions, aligns well with our observations of abrupt densification behaviour without detectable secondary phases by XRD post-sintering, supporting the proposed intrinsic transient liquid-phase-assisted densification mechanism.

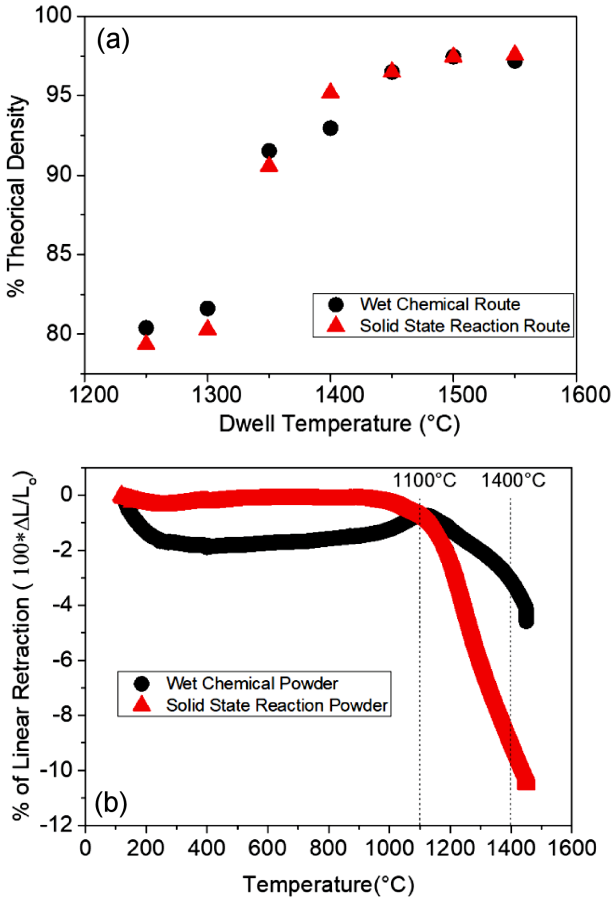

Figure 4. Densities of ceramic pellets sintered between 1250 and 1550 °C for 10 h (a) and linear shrinkage behaviour of green bodies measured by dilatometry (b)

3.3. Sintering mechanisms

Sintering theory indicates that densification in ceramic systems typically involves a combination of solid-state diffusion and liquid-phase mechanisms. Powders synthesized via wet chemical methods, characterized by fine particle size and high compositional homogeneity, predominantly densify through solid-state diffusion, requiring minimal transient liquid-phase assistance [11,29]. Conversely, powders obtained via solid-state reaction routes, involving oxides and carbonates, inherently exhibit larger particle sizes and lower compositional homogeneity, increasing their dependence on transient liquid-phase formation to achieve densification. Although this transient liquid phase is not introduced externally via additives, it arises intrinsically from local compositional deviations due to the partial BaO volatilization at high temperatures, as the dilatometric behaviour suggests. As this transient phase is strictly confined to high-temperature sintering condi-

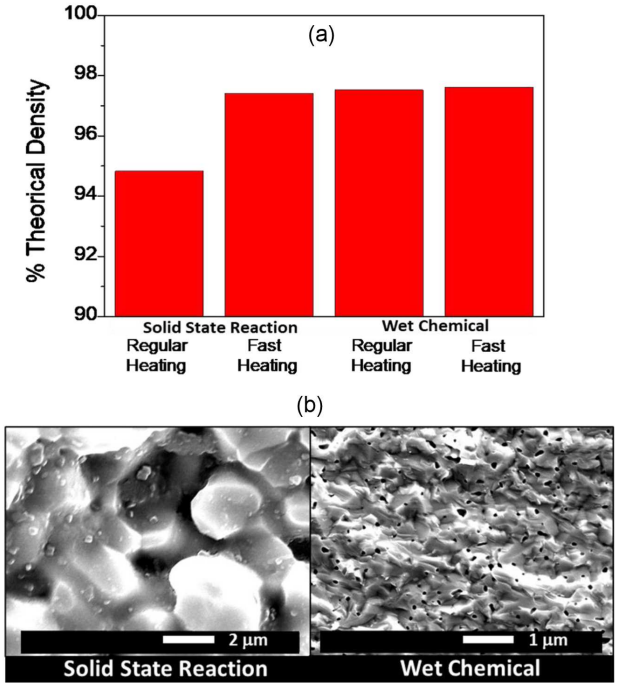

Figure 5. Relative densities of ceramic pellets prepared via solid-state reaction and wet chemical routes, sintered at 1550 °C for 1 h under regular and fast heating schedules (a) and SEM micrographs of samples sintered 1550 °C for 15 min under fast heating schedule (b)

tions, it does not persist in the sintered ceramics, aligning with the absence of detectable secondary phases by subsequent XRD analysis, as similarly documented by Ramos *et al.* [16].

Fast heating experiments were conducted to further elucidate the sintering mechanisms and densification behaviour. The ceramic pellets were sintered rapidly by heating to 1550 °C, holding for 15 min and 1 h, and immediately quenched to room temperature using a bottom-loading furnace. Densities of the fast heated sample and samples regularly sintered (1550 °C for 1 h) are compared (Fig. 5a). The results reveal comparable final densities for the ceramics prepared from the wet chemical powder and subjected to fast and regular heating schedules. However, rapid heating markedly enhanced densification efficiency of the solid-state reaction powders, suggesting that the regular heating rate, followed by a short dwell time of 1 h, may have led to incomplete formation or insufficient duration of the transient liquid phase, thereby limiting the achievable density compared to the fast heating rate.

The results presented on Fig. 5b demonstrate differences between the sintered samples obtained from two different powders and sintered by fast heating at 1550 °C for 15 min. The ceramics prepared from the wet chemical powder exhibits homogeneous, dense microstructure indicative of predominant solid-state diffusion mechanisms. In contrast, the ceramics derived from solid-state reaction powder exhibits microstructure with distinct spherical features at grain boundaries, indicative of incomplete sintering, resulting in reduced densification. This finding further emphasizes that the transient liquid-phase formation, as proposed in literature, is significantly more influential for solid-state reaction powders, a difference accentuated by the fast heating sintering experiments conducted in this study [16,31].

Microstructural differences between fractured surfaces of the sintered samples obtained from two different powders are shown in Fig. 6a. The ceramics prepared from the solid-state reaction powder display a more irregular and porous microstructure, especially at lower sintering temperature. The sintered samples obtained from wet chemical powder exhibit a denser and more uniform microstructure, consistent with their higher sinterability through solid-state diffusion mechanisms.

Figure 6b shows the SEM micrographs of polished surfaces of the dense samples obtained after thermal etching. The etching process successfully revealed the grain boundaries but also caused the exudation of distinct grains along the interface regions. At first, these exuded grains could be attributed to a secondary phase associated with impurities or a phase of different composition. However, SEM analysis using a backscattered electron detector revealed no compositional differences and the same exudation patterns for the ceramics obtained by both processing routes. Therefore, as described in the literature [11,16], the observed microstructures cannot be classified as secondary or impurity phases since they do not possess distinct chemical compositions from the matrix, which can explain their absence in the XRD patterns. In light of the previous discussion on liquid-phase-assisted sintering, these observations suggest that the exudation is associated with an intrinsic liquid phase formed during sintering. This phase, likely of stoichiometric composition, aids densification during sintering and is subsequently reincorporated into the grain boundaries. Since this final reincorporation step is inherently slow, the thermal etching process stimulates the exudation of this unstable liquid phase, resulting in the observed interface patterns. Microstructure evolution with increasing sintering temperatures (1450, 1500 and 1550 °C) further supports this interpretation.

Figure 7 presents SEM micrographs of fractured and polished/etched surfaces of the samples sintered for 1 h under regular and fast heating schedules. The fractured surfaces reveal key influences of two powder preparation methods. For the samples prepared by the solid-state reaction route, the fractured micrographs under fast heating display noticeable pores and small grains on the grain boundaries suggesting the exudation of a liquid phase during sintering. In contrast, a more uniform and dense microstructure characterizes the samples obtained by the wet chemical route, indicating that densification occurs predominantly through solid-state diffusion mechanisms.

The polished and thermally etched surfaces further support these observations. For the samples obtained

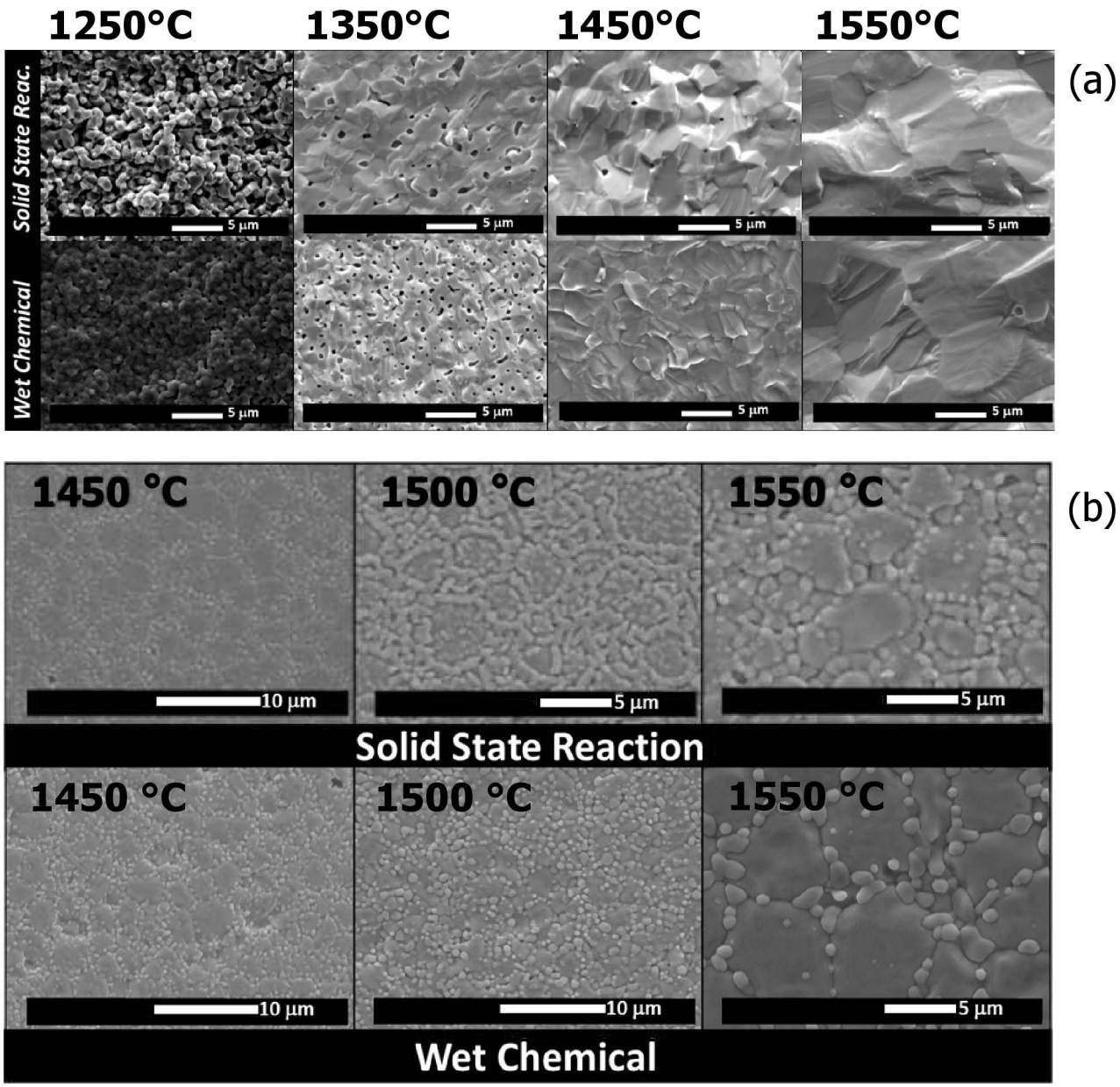

Figure 6. SEM micrographs of sintered samples (for 10 h) obtained from solid-state reaction and wet chemical powders: a) fractured sample surfaces and b) polished and thermally etched surfaces

from the solid-state reaction powder, the micrographs show regions of exudation, particularly along the grain boundaries, confirming the presence of a reincorporated liquid phase during sintering. This effect is more pronounced under the fast heating conditions, where the rapid temperature rise promotes liquid-phase formation but limits its complete reincorporation into the matrix. The etched surfaces of the ceramics obtained from wet chemical powder reveal well-defined grain boundaries with less pronounced exudation, further corroborating their low dependence on liquid-phase sintering.

These results confirm that the exudation behaviour is influenced by both the sintering schedule and the powder preparation route. Due to their fine particle size and high homogeneity, wet chemical powders exhibit higher sinterability with minimal reliance on intrinsic liquid-phase assistance. In contrast, the solid-state reaction powders, with lower sinterability, are more dependent on intrinsic liquid-phase formation.

3.4. Electrical characterization

The electrical conductivity of the sintered ceramics was investigated as a function of the processing route and sintering schedule. Figures 8a and 8b present the impedance spectra obtained at 150 °C for the ceramics prepared through wet chemical and solid-state reaction routes, sintered at temperatures between 1400 and 1550 °C. Bulk and grain boundary contributions are distinguishable in the impedance spectra. Figures 8c and 8d illustrate a distinct dependence of electrical conductivity on the sintering schedules for both powder preparation routes.

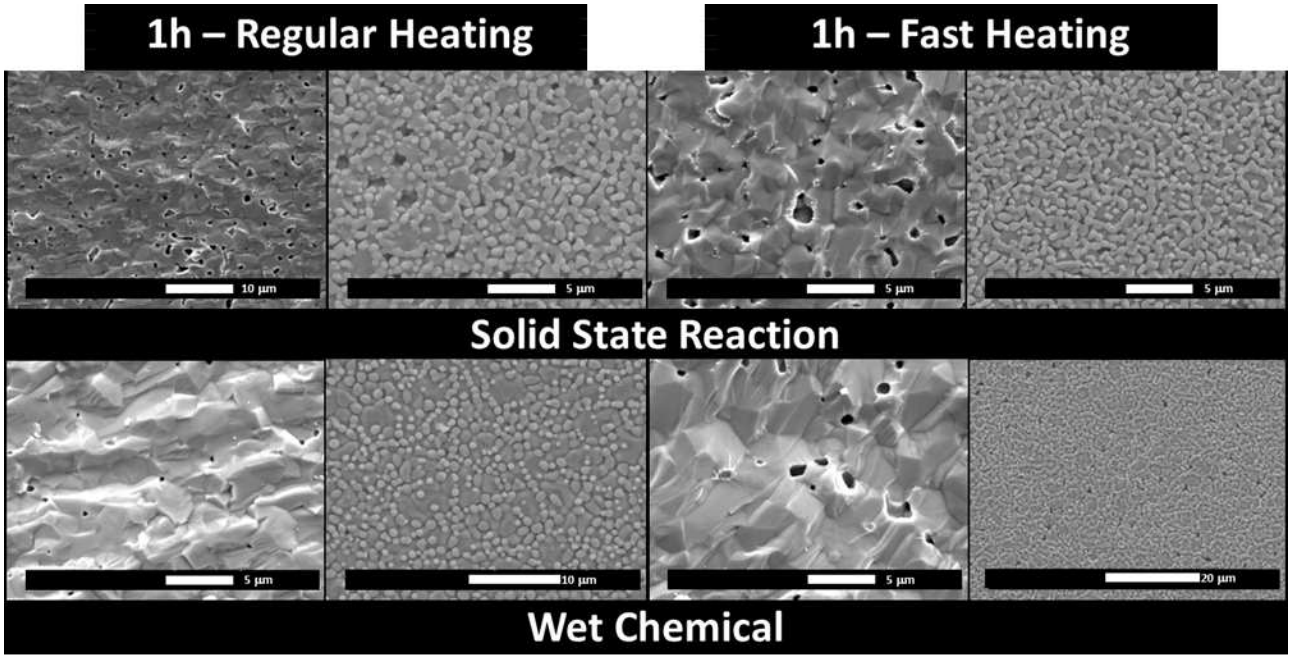

Figure 7. SEM micrographs of fractured surfaces (left) and polished/thermally etched surfaces (right) of samples sintered at 1550 °C for 1 h under regular and fast heating schedules

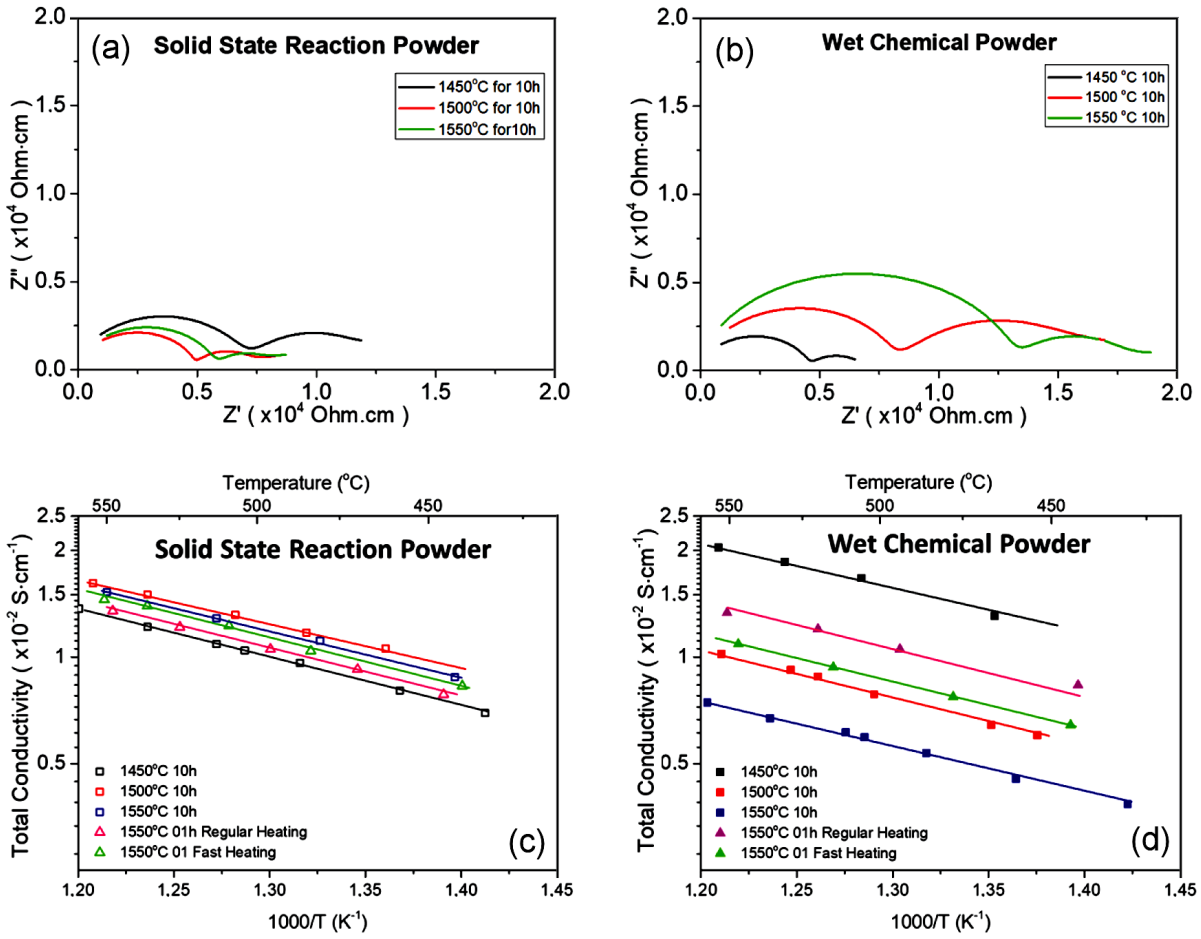

Figure 8. Impedance spectra at 150 °C for ceramics prepared via the solid-state reaction route sintered at 1450, 1500 and 1550 °C for 10 h (a, b) and electrical conductivities of ceramics prepared under different sintering schedule (c, d)

The ceramics prepared via the wet chemical route exhibits the highest conductivity values at the lowest sintering temperature (1450 °C) and the decrease in electrical properties was observed for the samples sintered at higher sintering temperatures and longer sintering time, indicating sensitivity to temperature-induced microstructural changes. Additionally, the ceramics prepared via the wet chemical route shows significant conductivity variations, which for example at 550 °C varies from 0.72×10^{-2} to 2.0×10^{-2} S/cm. On the other hand, the samples prepared via the solid-state reaction exhibit lower and more stable conductivity values, ranging from 1.3×10^{-2} to 1.5×10^{-2} S/cm at 550 °C. This distinct behaviour is attributed to the different sintering mechanisms discussed in the previous section. It is proposed that the stronger dependence on the transient liquid phase in the ceramics prepared from the solid-state reaction powder is responsible for their more homogeneous electrical properties across different sintering schedules. In contrast, the ceramics obtained from the wet chemical route exhibits high conductivity at lower sintering temperatures due to the reduced dependence on the transient liquid phase mechanism.

Although the literature indicates a strong correlation between electrical properties and subtle crystalline structural deviations, a detailed crystallographic investigation is beyond the scope of this paper. These results highlight distinct differences in conductivity behaviour between the ceramics obtained from two powders synthesized by different routes, underscoring the critical role of synthesis methods and sintering mechanisms in tailoring the electrical properties of $BaCe_{0.9}Y_{0.1}O_{3-\delta}$ ceramics.

IV. Conclusions

The sinterability and electrical properties of $BaCe_{0.9}Y_{0.1}O_{3-\delta}$ (BCY) ceramics processed through different powder synthesis routes and sintering schedules were investigated. The findings reveal a clear correlation between the processing method, the sintering mechanisms, and the resulting microstructural and electrical characteristics.

The wet chemical route demonstrated superior sinterability, favouring densification through solid-state sintering at lower temperatures and yielding higher electrical conductivity. However, these ceramics exhibited more significant variability in conductivity due to their sensitivity to temperature-induced microstructural changes. In contrast, the solid-state reaction route led to a more substantial reliance on transient liquid-phase sintering, producing a more uniform microstructure and lower, yet more consistent, electrical conductivity across different sintering conditions.

The competition between solid-state and liquid-phase sintering is evident, with lower sintering temperatures enhancing solid-state diffusion for the wet chemical route whereas higher temperatures and a solid-state reaction route promote liquid-phase-assisted densification.

Acknowledgements: For financial support, to Brazilian Research Councils (CNPq) and Federal Institute of Sao Paulo of Education, Science and Technology, to the Materials Engineering Department of the Federal University of Sao Carlos and Brazilian Center of Materials Research (CNPEM) for facilities and infrastructure.

References

1. J. Li, J. Cheng, Y. Zhang, Z. Chen, M. Nasr, M. Farghali, D.W. Rooney, P.-S. Yap, A.I. Osman, "Advancements in solid oxide fuel cell technology: bridging performance gaps for enhanced environmental sustainability", *Adv. Energy Sustain. Res.*, **5** [11] (2024) 2400132**.**
2. E.D. Wachsman, K.T. Lee, "Lowering the temperature of solid oxide fuel cells", *Science*, **334** [6058] (2011) 935–939.
3. C. Duan, J. Huang, N. Sullivan, R. O'Hayre, "Proton-conducting oxides for energy conversion and storage", *Appl. Phys. Rev.*, **7** [1] (2020) 011314.
4. P. Colomban, "Proton conductors and their applications: A tentative historical overview of the early researches", *Solid State Ionics*, **334** (2019) 125–144.
5. L.A. Omeiza, A. Kabyshev, K. Bekmyrza, K.A. Kuterbekov, M. Kubenova, Z.A. Zhumadilova, Y. Subramanian, M. Ali, N. Aidarbekov, A.K. Azad, "Constraints in sustainable electrode materials development for solid oxide fuel cell: A brief review", *Mater. Sci. Energy Technol.,* **8** (2025) 32–43.
6. D. Medvedev, "Trends in research and development of protonic ceramic electrolysis cells", *Int. J. Hydrogen Energy,* **44** [49] (2019) 26711–26740.
7. Y. Meng, J. Gao, Z. Zhao, J. Amoroso, J. Tong, K.S. Brinkman, "Review: recent progress in low-temperature proton-conducting ceramics", *J. Mater. Sci.*, **54** [13] (2019) 9291–9312.
8. D. Medvedev, A. Murashkina, E. Pikalova, A. Demin, A. Podias, P. Tsiakaras, "$BaCeO_3$: Materials development, properties and application", *Prog. Mater. Sci.,* **60** (2014) 72–129.
9. J. Kim, S. Sengodan, S. Kim, O. Kwon, Y. Bu, G. Kim, "Proton conducting oxides: A review of materials and applications for renewable energy conversion and storage", *Renew. Sustain. Energy Rev.,* **109** (2019) 606–618.
10. L. Bi, E. Traversa, "Synthesis strategies for improving the performance of doped-$BaZrO_3$ materials in solid oxide fuel cell applications", *J. Mater. Res.,* **29** [1] (2014) 1–15.
11. F.J.A. Loureiro, N. Nasani, G.S. Reddy, N.R. Munirathnam, D.P. Fagg, "A review on sintering technology of proton conducting $BaCeO_3$-$BaZrO_3$ perovskite oxide materials for protonic ceramic fuel cells", *J. Power Sources*, **438** (2019) 226991.
12. M. Amsif, D. Marrero-López, J.C. Ruiz-Morales, S. N. Savvin, P. Núñez, "The effect of Zn addition on the structure and transport properties of $BaCe_{0.9-x}Zr_xY_{0.1}O_{3-\delta}$", *J Eur. Ceram. Soc*, **34** [6] (2014) 1553–1562.
13. D.P. Guha, D. Kolar, "Phase equilibria in the system BaO-CeO_2", *J. Mater. Sci.,* **6** [9] (1971) 1174–1177.
14. J. Tong, D. Clark, M. Hoban, R. O'Hayre, "Cost-effective solid-state reactive sintering method for high conductiv-

ity proton conducting yttrium-doped barium zirconium ceramics", *Solid State Ionics*, **181** [11] (2010) 496–503.
15. D. Medvedev, V. Maragou, E. Pikalova, A. Demin, P. Tsiakaras, "Novel composite solid state electrolytes on the base of $BaCeO_3$ and CeO_2 for intermediate temperature electrochemical devices", *J. Power Sources*, **221** (2013) 217–227.
16. K. Ramos, L.P. Wendler, A.L. Chinelatto, A.A. Chinelatto, D.P.F. de Souza, "High-density $BaCe_{0.9}Y0.1O_{3-\delta}$ obtained by solid-state reaction sintered at 1200 °C without sintering aid", *J. Mater. Sci. Mater. Electron.*, **34** [3] (2023) 174.
17. L.P. Wendler, K. Ramos, D.M.P.F. Souza, "Investigation about the reason of limited grain growth of Y-doped barium zirconate", *Ceram. Int.*, **45** [15] (2019) 19120–19126.
18. Y.J. Gu, Z.G. Liu, J.H. Ouyang, F.Y. Yan, Y. Zhou, "Structure and electrical conductivity of $BaCe_{0.85}Ln_{0.15}O_{3-\delta}$ (Ln = Gd, Y, Yb) ceramics", *Electrochim. Acta*, **105** (2013) 547–553.
19. N.I. Matskevich, T. Wolf, M.Y. Matskevich, A.N. Bryzgalova, T.I. Chupakhina, I.V. Vyazovkin, "Synthesis and thermodynamic stability of new phase $BaCe_{0.6}Y_{0.3}In_{0.1}O_{2.8}$", *Thermochim. Acta*, **579** (2014) 22–26.
20. M. Amsif, D. Marrero-Lopez, J.C. Ruiz-Morales, S.N. Savvin, M. Gabás, P. Nunez, "Influence of rare-earth doping on the microstructure and conductivity of $BaCe_{0.9}Ln_{0.1}O_{3-\delta}$ proton conductors", *J. Power Sources*, **196** [7] (2011) 3461–3469.
21. M. Amsif, D. Marrero-López, J.C. Ruiz-Morales, S.N. Savvin, P. Núñez, "Effect of sintering aids on the conductivity of $BaCe_{0.9}Ln_{0.1}O_{3-\delta}$", *J. Power Sources*, **196** [22] (2011) 9154–9163.
22. S.H. Nien, C.S. Hsu, C.L. Chang, B.H. Hwang, "Preparation of $BaZr_{0.1}Ce_{0.7}Y_{0.2}O_{3-\delta}$ based solid oxide fuel cells with anode functional layers by tape casting", *Fuel Cells*, **11** [2] (2011) 178–183.
23. S. Yamaguchi, K. Nakamura, T. Higuchi, S. Shin, Y. Iguchi, "Basicity and hydroxyl capacity of proton-conducting perovskites", *Solid State Ionics,* **136-137** (2000) 191–195**.**
24. L. Spiridigliozzi, G. Accardo, E. Audasso, S.P. Yoon, G. Dell'Agli, "On the role of copper as a sintering aid in proton conducting Gd-doped barium cerate (BCGO)", *J. Alloys Compd.*, **960** (2023) 170762.
25. R.M. German, P. Suri, S.J. Park, "Review: Liquid phase sintering", *J. Mater. Sci.*, **44** [1] (2009) 1–39.
26. S.S. Che Abdullah, A. Rohaya, O. Nafisah, "Two-step sintering of fine barium cerate-zirconate ceramics electrolyte", *Key Eng. Mater.*, **594-595** (2014) 962–966.
27. K. Takeuchi, C.-K. Loong, J. W. Richardson, J. Guan, S.E. Dorris, U. Balachandran, "The crystal structures and phase transitions in Y-doped $BaCeO_3$: Their dependence on Y concentration and hydrogen doping," *Solid State Ion*, **138** [1] (2000) 63–77.
28. A. Subramaniyan, J. Tong, R.P. O'Hayre, N.M. Sammes, "Sintering studies on 20 mol% yttrium-doped barium cerate", *J. Am. Ceram. Soc.*, **94** [6] (2011) 1800–1804.
29. R.M. German, "Sintering with a liquid phase", pp. 247–303, Ch. 9 in *Sintering: from Empirical Observations to Scientific Principles*. Ed. R.M. German, Butterworth-Heinemann, Boston, 2014.
30. S. Loganathan, S. Biswas, G. Kaur, S. Giddey, "Role of sintering aids in electrical and material properties of yttrium- and cerium-doped barium zirconate electrolytes", *Processes*, **12** [10] (2024) 2278**.**
31. M. Yu, Q. Feng, Z. Liu, P. Zhang, X. Zhu, S. Mu, "Recent novel fabrication techniques for proton-conducting solid oxide fuel cells", *Crystals*, **14** [3] (2024) 225.